17th Australasian Fluid Mechanics Conference
Auckland, New Zealand
5-9 December 2010

The effect of incidence angle variation of a square cylinder on its dynamic response and wake states

J. Zhao[1], A. Nemes[1], D. Lo Jacono[1,2,3] and J. Sheridan[1]

[1]Fluids Laboratory for Aeronautical and Industrial Research (FLAIR)
Department of Mechanical and Aerospace Engineering
Monash University, Melbourne, Victoria, 3800 Australia

[2]Université de Toulouse; INPT, UPS; IMFT;
Allée Camille Soula, F-31400 Toulouse, France

[3]CNRS; IMFT; F-31400 Toulouse, France

Abstract

An experimental investigation has been carried out in a water channel on the transverse flow-induced vibration of a square cross-section cylinder at two different angles of incidence to the free-stream, $\alpha = 0^\circ$ (square) and 45° (diamond). The oscillation amplitude and frequency response of the cylinder were measured over a range of reduced velocity, U^*, and compared to the response of a circular cylinder. The phase of the lift force with respect to the cylinder's displacement was determined. Additionally, particle image velocimetry (PIV) was used to identify the transition of the wake structure from $2S$ to $2P$ mode for the diamond case. The results show that the square orientation follows a galloping response as expected, while the diamond behaves similarly to that of a circular cylinder undergoing vortex-induced vibration.

Introduction

Flow-induced vibration of a bluff body has been intensively studied in the past few decades due to its undesired impact on the fatigue life of structures, which can potentially lead to structural damage or catastrophic failure. This is critical in many engineering applications, such as flow around offshore risers, civil buildings and bridges. This subject has been reviewed extensively in [12].

Two typical body oscillators of flow-induced vibration are vortex-induced vibration (VIV) and galloping. Vortex-induced vibration occurs when the vortices alternatively shed from a bluff body result in fluctuating forces that cause the body to vibrate. A non-linear phenomenon known as synchronisation or "lock-in" occurs in VIV when the vortex shedding frequency matches the body oscillation frequency, and moves away from the Strouhal frequency, $St = f_{St}H/U$ (see [15] and [17]). Within this regime, the structure experiences large-amplitude oscillations or resonance if the frequencies are close to the natural frequency of the structure. Galloping is a movement-induced excitation that can be caused by aerodynamically unstable cross sections when the reduced velocity is above a critical value [12]. Like VIV, its behaviour is dependent on the damping and mass of the system, as well as the geometry [4]. Galloping can cause the structure to vibrate at much larger amplitudes than VIV, with a frequency many times lower than the shedding frequency.

Extensive studies have been conducted to investigate the fundamental characteristics of VIV of a circular cylinder. Reviews are given by [2], [17], and [16]. A pioneering study was conducted by Feng [5] in a wind tunnel, finding that the cylinder's oscillation frequencies lock on to the body's natural frequency, f_N, over a range of reduced velocity, $U^* = U/f_N L$, where U is the free-stream velocity and H is the projected cylinder width to the oncoming flow. More recent studies [9, 10] conducted experiments using an air-bearing rig with a water channel to provide very low values of the mass-damping parameter compared to that of Feng. Their results found that a three-branch amplitude response (labelled as "initial", "upper" and "lower" branches) occurred over the reduced velocity range, and that the synchronisation region extended to significantly higher velocities than observed by Feng, while not necessarily locked to the natural frequency of the structure. Experiments [7] have shown that the wake in the initial branch consists of two single vortices shed over one oscillation cycle of the body ($2S$ mode), while the upper and lower branch are associated with two pairs of vortices being shed ($2P$ mode).

Square cylinders undergoing oscillation have also been well studied, typically at zero angle of incidence and prone to galloping instability [1, 13, 14]. However, flow-induced vibration of a square cylinder with incidence angle variation has been investigated much less. In this paper, experimental results are presented on the transverse flow-induced vibration of a square cylinder at two different angles of flow incidence ($\alpha = 0^\circ$ and 45°).

Experimental Details

The experiments were conducted in the free-surface recirculating water channel of FLAIR in the Department of Mechanical and Aerospace Engineering at Monash University. The water channel facility has a test section of 6m in length, 0.6m in width, and 0.8m in depth.

The air bearing system was mounted on top of the water channel, allowing linear oscillatory movement of the cylinder transverse to the free-stream. The rigid cylinder model was made from a square-section aluminium tube with a side width of $D = 25$mm, wall thickness of 1.6mm and an immersed length of 740mm. It was vertically supported by the air bearing system, and elastically constrained by a pair of extension springs (LE014B13S, Lee Spring). The submerged end of the cylinder was within 2mm of the floor of the water channel. The total mass of the system undergoing oscillatory motion was $m = 1102$g, and the mass of the displaced water of the cylinder was $m_d = 462.1$g, giving a mass ratio of $m^* = m/m_d = 2.4$. Free decay tests were taken in air and in quiescent water to measure the natural frequencies of the structure and the system's damping ratio in air. The effective damping ratio in water was $\zeta = 5.4 \times 10^{-3}$, giving a low mass-damping ratio of $m^*\zeta = 0.013$.

The displacement of the cylinder was measured using a non-contact magnetostrictive linear variable differential transformer (LVDT: SE 750-10000, Macro Sensors, USA). The lift and drag forces acting on the cylinder were measured simultaneously us-

ing a two-component force balance based on strain gauges configured in Wheatstone bridge.

The near wake flow field of the cylinder was analysed using particle image velocimetry (PIV) technique. The flow was seeded with polyamide particles having a mean diameter of 55μm and a specific weight of 1.016g/m^3. Two miniature Ng:YAG pulse lasers (Continuum Minilite II Q-Switched lasers) produced a 2mm thick horizontal planar sheet, illuminating the particles in the plane of interest. Pairs of images were captured by a PCO 4000 (4008×2672pixel^2) CCD camera, equipped with a 105mm lens (Nikon Corporation, Japan). A second PIV system with a PCO Pixelfly camera (1392×1024pixel^2) was used for the free-stream velocity measurement. The PIV image data was analysed with in-house PIV software [6], using 32×32pixel^2 interrogation windows in a grid layout with 50% window overlap.

The PIV system's trigger TTL signal along with the position and force measurements were sampled at 100Hz by a National Instrument data acquisition system consisting of a NI PCI-6221 DAQ Board, a BNC-2110 Connector Block, and software LabVIEW 8.5. The recorded signals provided a time history of the location of the cylinder at the timing of each PIV image pair, allowing phase averaging of the PIV images based on the cylinder's position. At least 600 image pairs were taken at each U^* represented, providing over 70 image pairs at each of the eight phases. Frequencies were extracted using FFT, and confirmed with wavelet analysis [8].

Results

Experimental measurements were taken over a reduced velocity range with the square cylinder at two angles of flow incidence, $\alpha = 0^\circ$ and 45°. Amplitude response of the cylinder with $m^* = 2.4$ and $m^*\zeta = 0.013$ are shown in figure 1, and frequency response is shown in figure 2. Results are plotted alongside experimental data of a circular cylinder by [11] having a matching mass ratio, $m^* = 2.4$, and mass-damping ratio, $m^*\zeta = 0.013$. The amplitude, $A^*_{\max} = A_{\max}/H$, is the maximum amplitude recorded within the measurement time, $A_{\max}$, non-dimensionalised by the characteristic length of the cylinder, H, which is taken as the projected length facing the oncoming flow. The frequency response, f^*, is the frequency of oscillation, f, non-dimensionalised by the natural frequency of the structure, f_N, which is measured by free decay test in quiescent water in the present study.

Results for $\alpha = 45^\circ$

The amplitude of the $\alpha = 45^\circ$ case (diamond) follows the initial and upper branch behaviour of the circular cylinder, with a similar increase from an initial branch to an upper branch. The jump from the initial to upper branch, however, is not as high and occurs earlier, around $U^* = 3$. This is followed by a linear increase in amplitude to a maximum, $A^*_{\max} \approx 0.8$. Both diamond and circle cross sections attain a maximum amplitude near $U^* = 5.8$, before smoothly dropping off to a lower branch at $U^* = 7$.

The time histories in figure 3 show a synchronised frequency between the body's position and the lift force, and periodic sinusoidal motion with a noticeable variation in amplitudes of the body movement. The circular cylinder experiences a desynchronisation between the position and lift, visible in figure 1 by a drop in amplitude, from around $U^* = 10$ upwards. The amplitude for the diamond levels out at $A^* = 0.5$, but there is a breakdown in phase and periodicity evidentally at $U^* = 9$, as seen in the time history in figure 3 c).

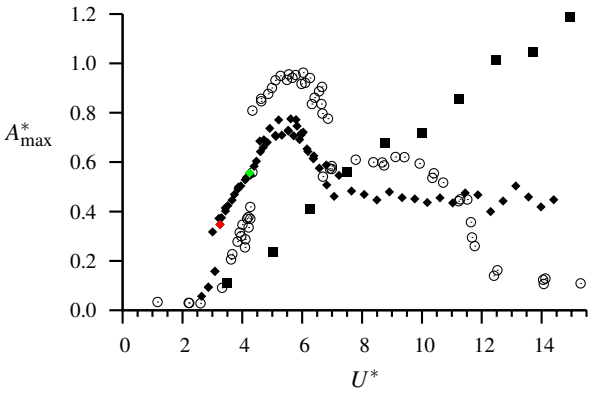

Figure 1: Effect of angle of incidence on behavioural response of maximum transverse amplitude, $A^*_{\max}$, of square section cylinder at $\alpha = 0^\circ$ (Square); at $\alpha = 45^\circ$ (Diamond) over a reduced velocity range, U^*, compared against [11](Circles). Red point is location of $2S$ wake mode (figure 4), green point represents $2P$ wake mode (figure 5).

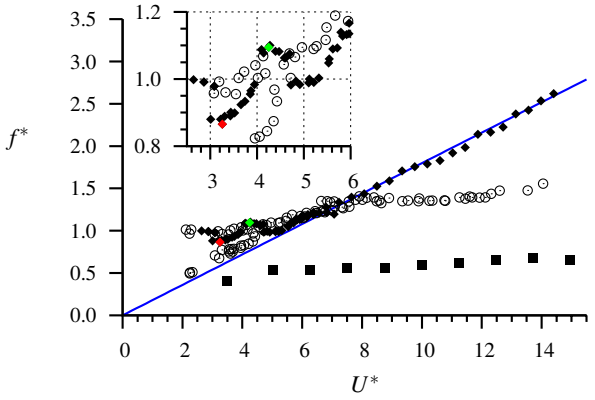

Figure 2: Effect of angle of incidence on behavioural response of frequency, f^*, of square section cylinder at $\alpha = 0^\circ$ (Square); at $\alpha = 45^\circ$ (Diamond) over a reduced velocity range, U^*, compared against [11] (Circles). The blue solid line represents the vortex shedding Strouhal curve for the diamond case, $St = 0.18$.

Figure 4 shows the $2S$ wake structure at the beginning of the upper branch. The vortex forming on the body rolls around the trailing edge of the diamond, and visibly separates into two vortices in the region of high strain near the sharp trailing edge (dashed contours around body). The smaller vortex merges in the near wake back into the larger one, and the single vortex travels downstream parallel to the flow forming a wake of width $2D$. As the reduced velocity is increased, the vortex formation changes in the region behind and around the trailing edge of the diamond, see figure 5, and the vortex is stretched and split at the trailing edge of the vortex into two (dashed contours), leading to a $2P$ wake mode. The wake widens to a width of $3D$. The greater interaction of the vortices and higher speed can account for what appears as faster diffusion of the vortices, although phase averaging of meandering vortices also have to be accounted for. The pairing of the vortices in the wake is difficult to quantify accurately due to their diffusion within $3D-5D$ downstream, however their position suggests outer and inner vortices of opposite signs begin to form a pair. The formation of the distinct $2P$ wake mode arises around amplitudes of $A^* = 0.5$, and is present in the upper and lower branch as U^* increases. The transition between $2S$ and $2P$ occurs over the U^* range $3.25-4.24$, and after the jump from the "initial" to "upper branch", suggesting two separate physical mechanisms

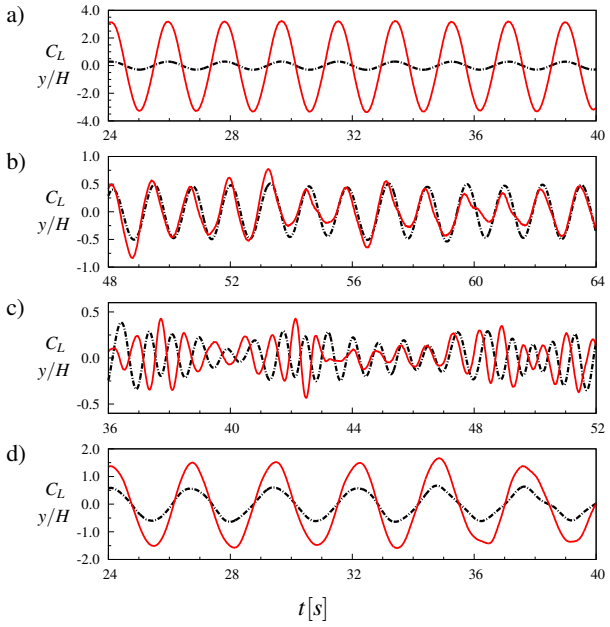

Figure 3: Time history of position, y/H, (black dot dashed line) and lift coefficient, $C_L = 2F_L/\rho U^2 HL$, (red solid line) for a) $\alpha = 45°$ at $U^* = 3.0$ - initial branch; b) $\alpha = 45°$ at $U^* = 6.80$ - upper branch; c) $\alpha = 45°$ at $U^* = 11.0$ - desynchronisation of phase between lift and position; d) $\alpha = 0°$ at $U^* = 10$.

are at play for the two responses.

The frequency response of the diamond in figure 2 shows that unlike the circular cylinder, there is no "lock-in" frequency to the body's natural frequency, and the oscillation frequency follows the vortex shedding frequency from $U^* = 5$, close to the peak of the upper branch. The lift generated by the vortex shedding and the body's position are in-phase over the initial, upper and lower branches until $U^* = 9$, at which point the phase at the shedding frequency moves in and out of phase between $\phi = 0 - 150°$, evident in the time histories in figure 3 c). The frequency response from the initial branch to the maximum of the upper branch follows a curious response: starting at a reduced oscillation frequency, f^*, near unity in the initial branch; then dropping slightly to $f^* = 0.9$ at the beginning of the upper branch; reaching a local maximum of $f^* = 1.1$ around $U^* = 4.3$; then decreasing again below unity until the amplitude peak of the upper branch; and from then following the vortex shedding frequency.

Results for $\alpha = 0°$

The square cylinder aligned at a $\alpha = 0°$ angle of incidence (square case) clearly does not follow a VIV response behaviour, and instead has a galloping-like response. The motion and lift both maintain a steady periodic signal over the entire velocity range. The amplitude response, A^*_{max}, in figure 1, linearly increases with reduced velocity, U^*, at an almost constant low frequency, f^*, seen in figure 2, in-phase with the vortex shedding through-out the reduced velocity range.

Discussion

It is evident that the angle of incidence of the square cylinder determines the type of flow-induced vibration it undergoes. This extra parameter for the geometry breaks the symmetry with respect to the cylinder's spanwise axis, and can be used to catalogue the flow behaviour. As it is varied, the discontinuity along the body of the square cylinder also varies the location of the

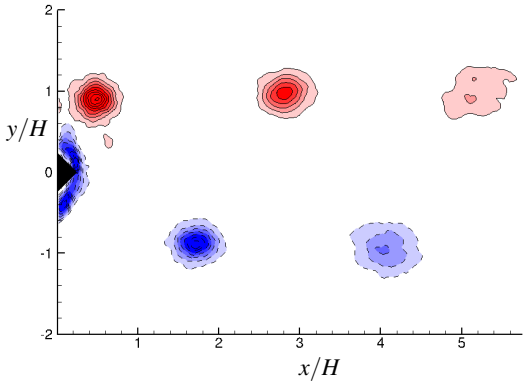

Figure 4: Vortex shedding behind the diamond cross section at $U^* = 3.25$. The body encourages the shed vortex to be split, however it rejoins close to body. The wake formation is two singular rows of opposite signed vortices forming a wake over $2D$ wide.

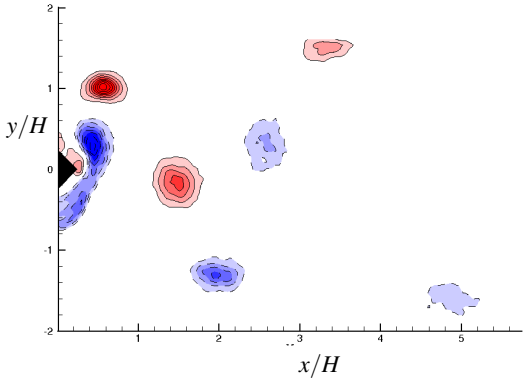

Figure 5: Vortex shedding behind the diamond cross section at $U^* = 4.24$. The vortex around the body separates around the end point of the diamond, and two distinct vortices propagate into the wake. The wake formation contains 2 vortex pairs of opposite sign per shedding cycle. The wake width extends $1.5D$ on each side of the center-line.

separation points. For the square orientation one face is normal to the oncoming flow, with separation around the two leading edges causing a much wider separation region and wake region to develop than seen in the circular geometry or diamond orientation. The frequency of the oscillations does not "lock-in" to the body's natural frequency, nor does it follow the Strouhal relationship curve, instead exhibiting a very low constant frequency, showing that the vortex shedding matches the galloping frequency not the natural Strouhal frequency.

In stark contrast, the diamond orientation frequency response fluctuates around $f^* = 1$ in the initial branch region, and from around $U^* = 5$, when the upper branch has reached its maximum, the non-dimensionalised frequency increases linearly with reduced velocity along the vortex shedding Strouhal curve, $St = 0.18$. It suggests that at low U^* the motion locks to the natural frequency of the body, and as U^*increases the frequency is influenced by the increased amplitude increasing the effective angle of incidence. The amplitude behaviour however, is nevertheless clearly very similar to the VIV response of the circular cylinder. The orientation of the geometry to the flow, and the location of the separation points appear to provide the conditions for the vortices to drive the body oscillations at its shedding frequency. This deviates from the circular cylinder response, which sees its own non-classical phenomena with the oscilla-

tion moving away from the body's natural frequency. This has been attributed to low mass-damping [11].

Up until $U^* = 9$, the oscillation and lift frequencies are locked in-phase. It is interesting that although there is a phase desynchronisation between lift and position, the frequency of oscillation continues to match the shedding frequency and follows the Strouhal curve. For higher reduced velocities, the phase shifts irregularly between $\phi = 0 - 150^\circ$.

The other significant deviation from the circular cylinder results for the diamond case occurs in the wake response. The transition for $2S$ to $2P$ is seen in circular cylinder studies to occur at the transition from lower to upper branch [3, 7], whereas for the diamond case the transition occurs after the amplitude jump.

Conclusions

Flow-induced vibration of a square cylinder with angle variation of flow incidence was experimentally studied. Results were compared to the circular cylinder, the canonical geometry for VIV studies. Results have demonstrated that by breaking one symmetry through the introduction of the angle of incidence parameter, α, the type of flow-induced vibration experienced can be influenced.

The square orientation exhibited a galloping type response over the reduced velocity range of $U^* = 5 - 15$ as expected, maintaining a low frequency of oscillation with a linear increase in amplitude to reduced velocity. There was no visible influence of the vortex shedding on frequency selection or amplitude, in fact, the shedding matched the low frequency of oscillation.

The diamond orientation exhibited a VIV response over the same velocity range, matching the amplitude response of a circular cylinder, with initial, lower and upper branches evident, and the wake mode transition from $2S$ to $2P$ was found. The maximum amplitudes were lower in the upper and lower branches than the circular cylinder results, but transition between branches coincided well with the reduced velocities of those seen in the transitions of the circular cylinder case. The breakdown in periodicity and phase in the lower branch at $U^* = 9$ showed no effects on frequency or amplitude response, maintaining a constant amplitude and matching the shedding frequency, and matched the reduced velocity where the circular cylinder reaches desynchronisation.

The study also demonstrated the separate behaviour of amplitude response and wake modes as compared to circular cylinder VIV, highlighting the strong effect geometry has on the physics in the coupling between the fluid and body.

In the current study, both angles of incidence studied maintained the horizontal and vertical symmetry of the square cross-section. It is reasonable to expect that a variation of the angle of incidence, α, to an asymmetric angle will, having broken both symmetries, bring about a change in response behaviours, and a combination of VIV and galloping behaviour could be induced.

Acknowledgements

J. Zhao would like to acknowledge the support of a Monash Departmental Scholarship (MDS) from Department of Mechanical and Aerospace Engineering, Monash University, and the support from ARC Discovery (DP0774525).

References

[1] Bearman, P., Gartshore, I., Maull, D. and Parkinson, G., Experiments on flow-induced vibration of a square-section cylinder, *Journal of Fluids and Structures*, **1**, 1987, 19–34.

[2] Bearman, P. W., Vortex shedding from oscillating bluff bodies, *Annual Review of Fluid Mechanics*, **16**, 1984, 195–222.

[3] Carberry, J., Govardhan, R., Sheridan, J., Rockwell, D. and Williamson, C. H. K., Wake states and response branches of forced and freely oscillating cylinders, *European Journal of Mechanics - B/Fluids*, **23**, 2004, 89–97.

[4] Corless, R. and Parkinson, G., A model of the combined effects of vortex-induced oscillation and galloping, *Journal of Fluids and Structures*, **2**, 1988, 203–220.

[5] Feng, C. C., *The measurements of vortex-induced effects in flow past a stationary and oscillating circular and D-section cylinders.*, Master's thesis, University BC, Vancouver, Canada, 1968.

[6] Fouras, A., Lo Jacono, D. and Hourigan, K., Target-free stereo piv: a novel technique with inherent error estimation and improved accuracy, *Experiments in Fluids*, **44**, 2008, 317–329.

[7] Govardhan, R. and Williamson, C. H. K., Modes of vortex formation and frequency response of a freely vibrating cylinder, *Journal of Fluid Mechanics*, **420**, 2000, 85–130.

[8] Grinsted, A., Moore, J. C. and Jevrejeva, S., Application of the cross wavelet transform and wavelet coherence to geophysical time series, *Nonlinear Processes in Geophysics*, **11**, 2004, 561–566.

[9] Khalak, A. and Williamson, C. H. K., Dynamics of a Hydroelastic Cylinder With Very Low Mass and Damping, *Journal of Fluids and Structures*, **10**, 1996, 455–472.

[10] Khalak, A. and Williamson, C. H. K., Fluid Forces and Dynamics of a Hydroelastic Structure With Very Low Mass and Damping, *Journal of Fluids and Structures*, **11**, 1997, 973–982.

[11] Khalak, A. and Williamson, C. H. K., Investigation of the relative effects of mass and damping in vortex-induced vibration of a circular cylinder, *Journal of Wind Engineering*, **67-71**, 1997, 341–350.

[12] Naudascher, E. and Rockwell, D., *Flow-induced vibrations: an engineering guide*, Dover Publications, 2005.

[13] Norberg, C., Flow around rectangular cylinders: pressure forces and wake frequencies, *Journal of Wind Engineering and Industrial Aerodynamics*, **49**, 1993, 187–196.

[14] Parkinson, G. and Brooks, N., On the aeroelastic instability of bluff cylinders, *Journal of applied mechanics*, **28**, 1961, 225–258.

[15] Sarpkaya, T., Hydrodynamic damping, flow-induced oscillations, and biharmonic response, *Journal of Offshore Mechanics and Arctic Engineering*, **117**, 1995, 232.

[16] Sarpkaya, T., A critical review of the intrinsic nature of vortex-induced vibrations, *J. Fluids Struct.*, **19**, 2004, 389–447.

[17] Williamson, C. H. K. and Govardhan, R., Vortex-Induced Vibrations, *Annual Review of Fluid Mechanics*, **36**, 2004, 413–455.